Nanotechnology **17** (2006) 5652–5658 | doi:10.1088/0957-4484/17/22/020

Determination of the strain generated in InAs/InP quantum wires: prediction of nucleation sites

S I Molina[1,2], T Ben[1], D L Sales[1], J Pizarro[3], P L Galindo[3], M Varela[2], S J Pennycook[2], D Fuster[4], Y González[4] and L González[4]

[1] Departamento de Ciencia de los Materiales e I.M. y Q.I., Facultad de Ciencias, Universidad de Cádiz, Campus Río San Pedro, s/n, 11510 Puerto Real, Cádiz, Spain
[2] Condensed Matter Sciences Division, Oak Ridge National Laboratory, Oak Ridge, TN 37831, USA
[3] Departamento de Lenguajes y Sistemas Informáticos, CASEM, Universidad de Cádiz, Campus Río San Pedro, s/n, 11510 Puerto Real, Cádiz, Spain
[4] Instituto de Microelectrónica de Madrid (CNM, CSIC), Isaac Newton 8, 28760 Tres Cantos, Madrid, Spain

E-mail: sergio.molina@uca.es and molina@ornl.gov

Received 23 August 2006, in final form 30 September 2006
Published 30 October 2006
Online at stacks.iop.org/Nano/17/5652

Abstract
The compositional distribution in a self-assembled InAs(P) quantum wire grown by molecular beam epitaxy on an InP(001) substrate has been determined by electron energy loss spectrum imaging. We have determined the strain and stress fields generated in and around this wire capped with a 5 nm InP layer by finite element calculations using as input the compositional map experimentally obtained. Preferential sites for nucleation of wires grown on the surface of this InP capping layer are predicted, based on chemical potential minimization, from the determined strain and stress fields on this surface. The determined preferential sites for wire nucleation agree with their experimentally measured locations. The method used in this paper, which combines electron energy loss spectroscopy, high-resolution Z contrast imaging, and elastic theory finite element calculations, is believed to be a valuable technique of wide applicability for predicting the preferential nucleation sites of epitaxial self-assembled nano-objects.

1. Introduction

The growth of self-assembled InAs nanostructures on InP(001) substrates leads to the formation of InAs(P) quantum dots or wires. The growth of quantum dots has been an approach widely investigated, both for the InAs/InP system [1–4] and for other heteroepitaxial material systems [5]. However, some groups [6–9] have demonstrated that the controlled epitaxial growth of InAs quantum wires on InP substrates is another valuable approach to fabricate materials emitting in infrared wavelengths of interest for telecommunications. It is worth mentioning that these wires are grown epitaxially on the substrate surface, in contrast to other wires investigated for many authors [10, 11], which are vertically grown upward from the substrate. As a consequence of the intensive research carried out on this type of wire during the last few years, a good understanding of the growth mechanism responsible for their formation and the dependence on their structural and photoluminescence properties on the growth parameters has been achieved [12–15]. In fact, the control of the growth process of these nanowires allows us to produce materials with emitting wavelengths in the range 1.2–1.9 μm [13].

These wires can be stacked to increase their density and organization degree. Their optical quality can also be improved if the sizes of the stacked wires are similar. The knowledge of the effect of stress field associated to each grown wire on the

size of upper stacked wires allows us to improve the uniformity of the wire sizes and therefore to improve the optical quality of the quantum wire stacked layers. Two critical parameters that help to change the size of the stacked wires are the thickness and the growth temperature of the InP spacing layer between a couple of adjacent stacks. Recently we have reported the effect of the inhomogeneous stress fields associated to the grown wires on the stacking of InAs/InP(001) quantum wires based on a combined study by *in situ* stress measurements and transmission electron microscopy [14]. We explained the formation of wires in correlated stacked layers by considering stress driven mass transport and P/As exchange.

In this work, we have determined the strain in an InP cap layer grown on an InAs(P) wire layer deposited by molecular beam epitaxy (MBE) on an InP(001) substrate, from the analysis of high-resolution Z contrast and electron energy loss spectrum imaging results together with finite element calculations. The determined strain values and our previous knowledge on the stacking of the wires capped by an InP layer allowed us to predict the nucleation sites of stacked wires.

2. Experimental details

A layer of InAs wires was grown by solid-source MBE on an InP(001) substrate by deposition of 2.5 monolayers (ML) of InAs at 0.1 ML s^{-1}, growth temperature of 515 °C and As_4 beam equivalent pressure of 2.3×10^{-6} mbar. After the formation of the wires, a cap layer of 20 nm of InP was grown at 380 °C by atomic layer MBE at 1 ML s^{-1}. The grown wires are oriented along $[1\bar{1}0]$ and periodically arranged along [110]. We will call this epitaxial material sample A.

The composition in one of these wires was determined by spatially resolved electron energy loss spectroscopy (EELS) with a dedicated aberration corrected VG HB501 scanning transmission electron microscope. The analysed wire was also imaged by high-resolution scanning transmission electron microscopy (STEM) using a high-angle annular dark field (HAADF) detector in the dedicated aberration corrected VG HB501 microscope, with probe size of 0.13 nm.

Specimens were prepared for STEM studies by following standard procedures (mechanical and ion milling thinning) to minimize the damage to the InP during the preparation process. Electron transparency was obtained with a precision ion polishing system (PIPS) at up to 3 kV and 4° of beam tilt.

EELS spectrum images were acquired with energies between the zero-loss peak and 404 eV. The As M (41 eV), In N (41 eV), P L (132 eV) and C K (284 eV) edges were registered simultaneously. The C signal was relatively low, showing very little contamination. The P L edge was used for quantification purposes. Elemental maps of P were obtained by first performing a background subtraction (power-law fit) using a window between 107 and 127 eV, then integrating the P signal between 131 and 141 eV and dividing it by the integrated background between 117 and 127 eV. In some sense, this is equivalent to the three-window technique widely used in energy-filtered transmission electron microscopy (EFTEM). Thickness maps (t/λ) showed that the specimen thickness in the area was very homogeneous and around 0.9 inelastic mean free paths.

3. Measurement of the composition in a quantum wire

Self-assembled quantum wires formed by deposition of InAs on InP and capped by an InP layer are actually constituted by the alloy $InAs_xP_{1-x}$. The compositional distribution in the wire was determined from EELS spectrum imaging (SI). The P composition in the wire was imaged by analysing the P signal contained in the corresponding spectra. The original P map obtained from the EELS spectra consists of intensity (greyscale) values ranging from 0 to 255 which represent the P composition. The obtained P map is shown in figure 1(a). Darker intensities of this image correspond to As-rich regions. The high-resolution Z contrast image of figure 1(b) corresponds to the same wire analysed by EELS SI. In good agreement with the compositional map determined by EELS SI, an enrichment of As towards the inner part of the wire is evidenced from the Z contrast image. This fact is clearly seen in the intensity profile of the HAADF image of the wire represented in figure 2. An increase of the electrons collected by the high-angle aperture is measured in the inner part of the wire. This increase corresponds to an increase of the Z number, and therefore of the As content, as $Z(\mathrm{As}) = 33$ is larger than $Z(\mathrm{P}) = 15$.

A low-pass filter was applied to the image of figure 1(a) to reduce the noise associated to higher spatial frequencies. Assuming that the phosphorous composition outside the wire (in the InP material below and over the wire) is 100%, the value of each pixel in the P map is taken as a reference value corresponding to 0% As in these pure InP regions. To find the As composition of each pixel, the value of each pixel is linearly recalculated taking into account the InP reference values. Slight variations of the reference values exist for different regions of the pure InP regions, mostly associated to local specimen thickness changes. To minimize this effect, a plane was fitted using data from the pure InP regions of the P map. The resulting As map is shown in figure 3(a). For visualization purposes, figure 3(b) shows a magnified picture of the wire compositional distribution after applying a strong Gaussian filter. This image shows the existence of an As compositional asymmetry in the wire. As we will show in the following, this compositional asymmetry in the wires has a strong influence on the position of the subsequent wires in the stacked wire layers.

4. Determination of the stress and strain in an InP layer capping an InAs(P) quantum wire

4.1. Distribution of stacked quantum wires

In previous works [14, 15], the mechanism of wire formation and the arrangement of stacked wires (grown in similar conditions to the single wire layer studied in this paper) were studied as a function of the InP spacing layer thickness that separates each stack from the next one. It was concluded that the dependence of the degree of alignment in the arrangement of the stacked wires on the InP spacing layer thickness is due to the strain field generated around each nanowire. This dependence was qualitatively demonstrated in those articles.

In particular, in samples consisting of six stacked wire layers, the majority of the stacked wires distribute almost

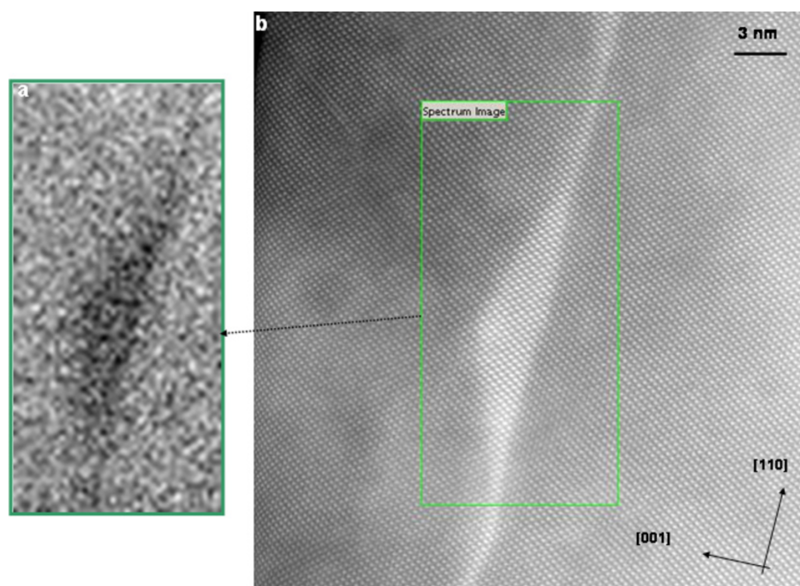

Figure 1. (a) P compositional map obtained from the analysis of the EELS spectra obtained in the wire imaged by high-resolution Z contrast (in a VG HB501) in part (b).

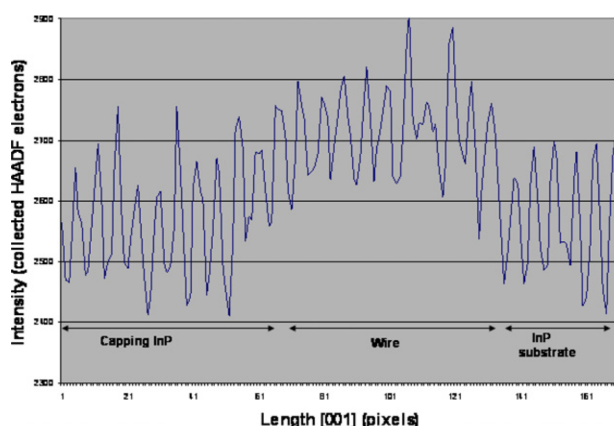

Figure 2. Intensity profile along [001] of the central part of the Z contrast image of 1(b). The locations of the capping InP, wire and InP substrate are labelled.

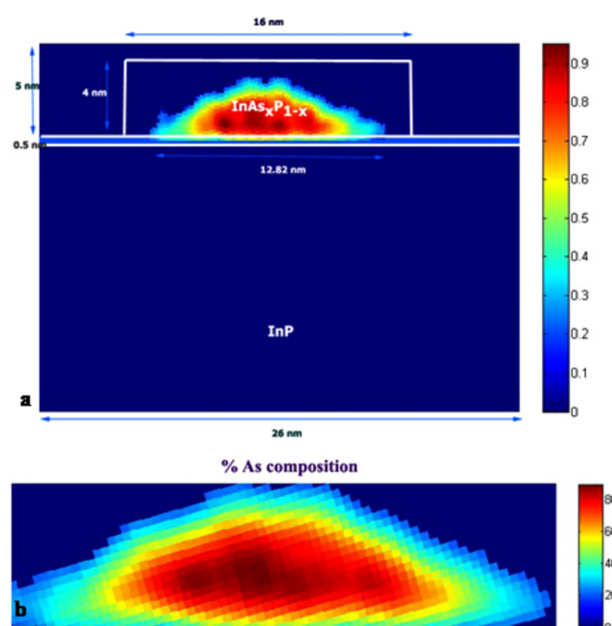

Figure 3. (a) Arsenic compositional map of the wire determined from the EELS spectra. (b) Magnified image of the As compositional distribution in the wire. The width of the wire is 12.8 nm and its height is 3.2 nm.

vertically when the InP spacing layer thickness is 5 nm. For samples with larger spacing layer thicknesses the ordering of the stacked wires is reduced and a completely random distribution of stacked wires is obtained for InP spacing layers of 20 nm.

Figure 4 shows the typical arrangement of wires in a sample consisting of six stacked wire layers (only three are represented in the drawing) with 5 nm of InP spacing layer thickness. This arrangement was determined from a detailed study of TEM and HRTEM images that have been reported in previous publications. In this figure we can observe how the stacked wires are distributed along the stacking sequence. We define α as the angle formed between [001] and the straight line which passes through the centre of the base of a wire in the first layer of wires and the centre of the base of the closest wire in the second stacked layer of wires. The mean value of α is 9° and its standard deviation is 5°.

As shown before (see figure 3), the composition distribution of As (and P) in a wire (sample A) is slightly asymmetrical. If the As compositional distribution in the wires were perfectly symmetrical, the strain field generated on the InP capping layer would have a maximum value just on top of the centre of this wire, because the composition profile has a maximum in its central part. An increase of As means a larger percentage of InAs in the alloy and therefore the capping InP will grow more strained on the InAs-rich places. If this

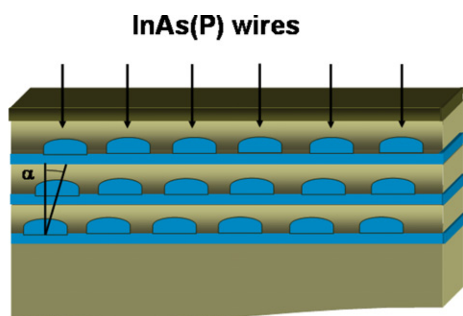

Figure 4. Arrangement of stacked wires in a sample with 5 nm of InP spacing layer thickness. The definition of the angle α, that quantifies the tilting of the stacking of the wires, is given in this figure.

(This figure is in colour only in the electronic version)

were exactly our case, the strain and surface shape, as we will explain in more detail later, would favour the nucleation of stacked wires just in the centre of the top of the wire underneath.

The real situation is that a slight asymmetry exists in the As composition of the wire. We can predict that this fact will motivate a displacement of the ε_{xx} maximum and the ε_{zz} minimum to another zone slightly shifted from the top of the centre of the wire underneath, and hence the nucleation of the upper stacked wire will be somewhat displaced with respect to the symmetrical case.

4.2. Determination of stress and strain fields by the finite element method

In the following we will quantify this displacement by finite element calculation of the three-dimensional (3D) strain distribution using a compositional model for the $InAs_xP_{1-x}$ wire grown on InP substrate extracted from the experimental asymmetrical compositional map. The 3D model was defined taking into account the elastic parameters, composition and boundary conditions of the materials obtained from the EELS and high-resolution Z contrast results.

Composition. The composition values corresponding to the wire and wetting layer were directly taken from the As map obtained from the spatially resolved EELS spectra. Note that the As composition will be different depending on x (coordinate along [110], this is, transversal direction to the wire) and z (coordinate along [001]) coordinates. The capping layer and substrate were assumed to be pure InP.

Boundary conditions. A 3D wire was modelled and the symmetries were then incorporated into the calculations to represent the entire sample. The periodicity of the structure was chosen to be 26 nm and it was taken into account by applying the appropriate boundary condition: all the nodes of symmetry planes were fixed against displacement in the directions normal to these planes. This periodicity corresponds to the average value measured by transmission electron microscopy.

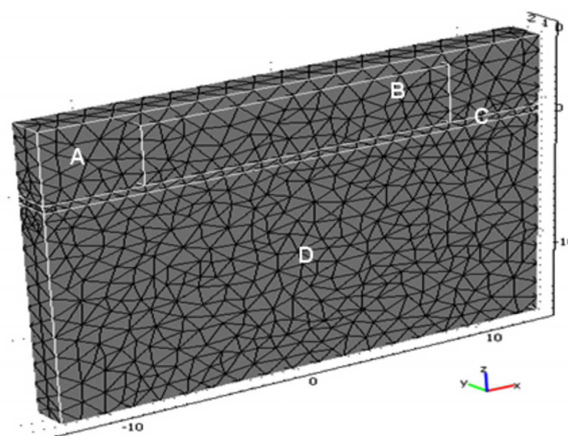

Figure 5. Illustration of the mesh used in the 3D finite element calculation. Four regions are defined in the model: (A) InP capping layer, (B) rectangular prism where $InAs_xP_{1-x}$ wire is included, (C) wetting layer and (D) InP substrate. Dimensions of each region: (A) 26 nm × 5 nm × 2 nm; (B) 16 nm × 4 nm × 2 nm; (C) 26 nm × 0.5 nm × 2 nm; (D) 26 nm × 15 nm × 2 nm.

Elastic parameters. Anisotropic linear elastic behaviour was considered. Elastic properties were taken from [16].

We built up the basic mesh represented in figure 5 for 3D finite element calculation. Four regions constitute the model represented in this figure: region A corresponds to InP capping layer, B is a rectangular prism that includes the $InAs_xP_{1-x}$ wire region, C is the wetting layer and D corresponds to the InP substrate. These regions constituting the mesh are superimposed on the experimentally obtained As map in figure 3(a). The wetting layer thickness is two monolayers. The substrate thickness was chosen large enough (15 nm) so that a further increase does not influence the results. The unstructured mesh generator is based on the Delaunay algorithm and can be used for all geometry objects.

Vegard's law was assumed for the determination of $InAs_xP_{1-x}$ elastic constants and lattice parameters. To introduce the misfit at the interface between layer and substrate, initial strain was assumed to be $\varepsilon_0 = (a_{InAs_xP_{1-x}} - a_{InP})/a_{InP}$, being therefore dependent on the As concentration.

Figure 6 presents the resulting strain components determined by introducing the realistic (asymmetrical) compositional model of the wire represented in figure 3. From the analysis of the strain results represented in figure 6 we can confirm the existence of the predicted displacement of the ε_{xx} maximum and the ε_{zz} minimum to another zone slightly farther away from the top of the centre of the wire underneath. The absolute value of the determined displacement is 0.86 nm, which corresponds to an angle of 9.8° between [001] and the straight line joining the position of the critical strains point at the growth surface of the 5 nm InP capping layer with the centre of the base of the studied wire in the first layer, in good agreement with the values of α experimentally observed (the average experimental value of α is 9°).

In figure 7 we show the corresponding stress profiles. We observe the existence of a maximum of the x [110] component of the stress (σ_{xx}) of 0.7 GPa in the same location as the above-mentioned critical strains. This value is close to the one calculated assuming a compositionally symmetrical

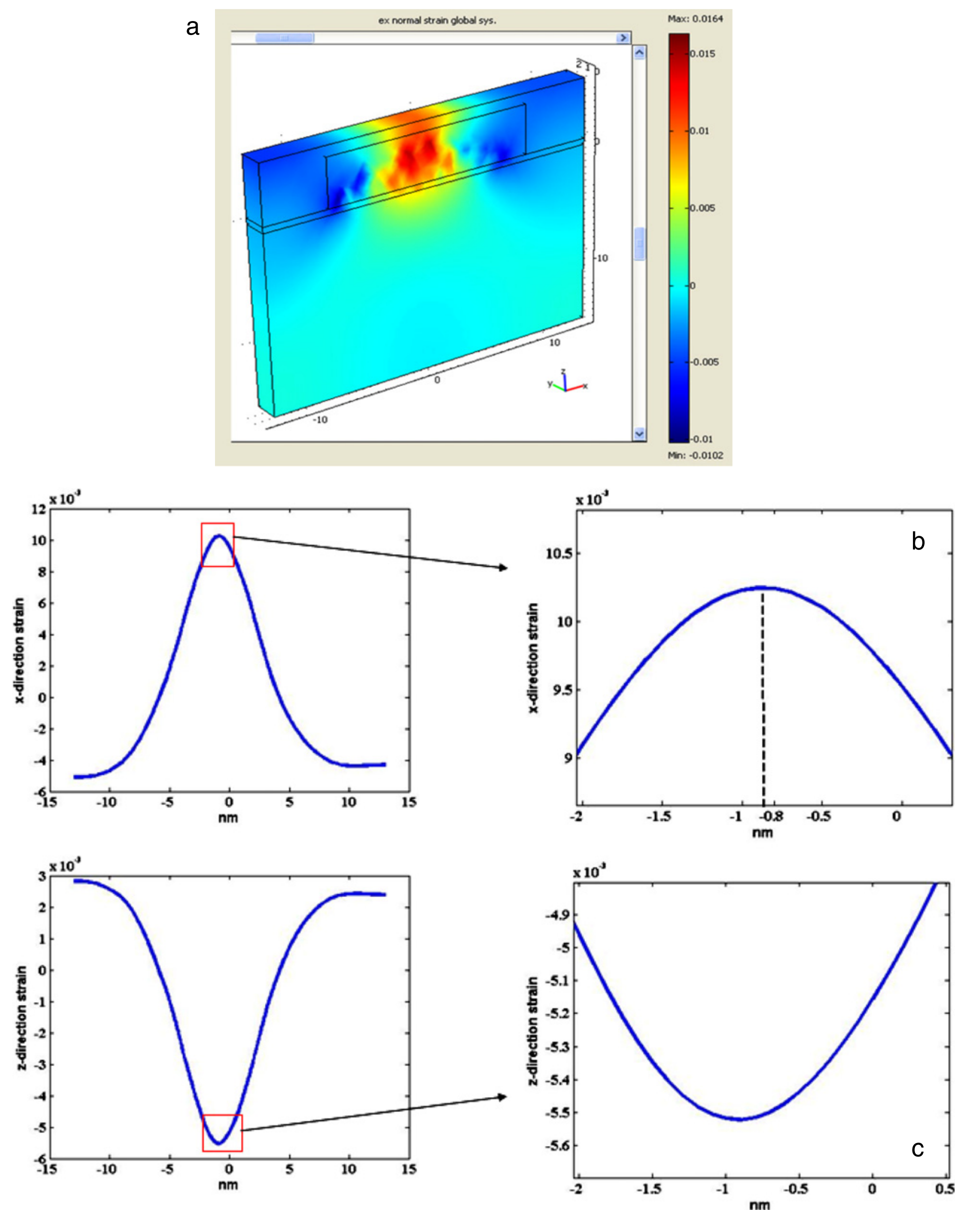

Figure 6. (a) 3D representation of the x [110] component of the strain (ε_{xx}) obtained by finite element calculations. Profiles of the ε_{xx} and ε_{zz} ([001] component of the strain) values versus x obtained at the surface of the 5 nm thick InP capping layer are shown in (b) and (c) respectively. The 0 nm point in the abscissa axis corresponds to the centre of the wire underneath. $x = [110]$; $y = [1\bar{1}0]$; $z = [001]$.

wire, though the location of this maximum in this case is not displaced from the centre of the wire underneath. This is, the asymmetry of the composition in the wire does not affect the stress magnitude much but it significantly affects its distribution on the surface of the InP layer capping the wire.

5. Location of preferential nucleation sites for quantum wires

In order to find the location at the surface of the 5 nm InP capping layer where the nucleation of wires of the second stacked layer will take place, we have to determine those surface zones where the chemical potential is minimized. The chemical potential μ can be evaluated as $\mu = \mu_0 + \mu_E + \mu_S + \mu_M$, where μ_0 is the chemical potential of a flat and unstressed surface, μ_E counts the effect of the elastic energy on the chemical potential, μ_S evaluates the influence of the surface energy and therefore it depends on the surface curvature [17], and μ_M is the chemical potential component associated to the entropy of mixing of the formed alloy [18], that is, it depends on the composition of the formed alloy. In our case, μ_M can be considered to be independent on the surface site because the whole surface consists of the binary compound InP. Therefore the two terms of the chemical potential that will contribute to create preferential sites to nucleate wires on the InP surface are μ_E and μ_S. The term μ_E will be minimized for those surface zones where the elastic energy is minimum for the initial growth of InAs, this is, where ε_{xx} and σ_{xx} have maximum values for InP at the growth surface. On the other hand, the term μ_S will be minimized for the concave surface

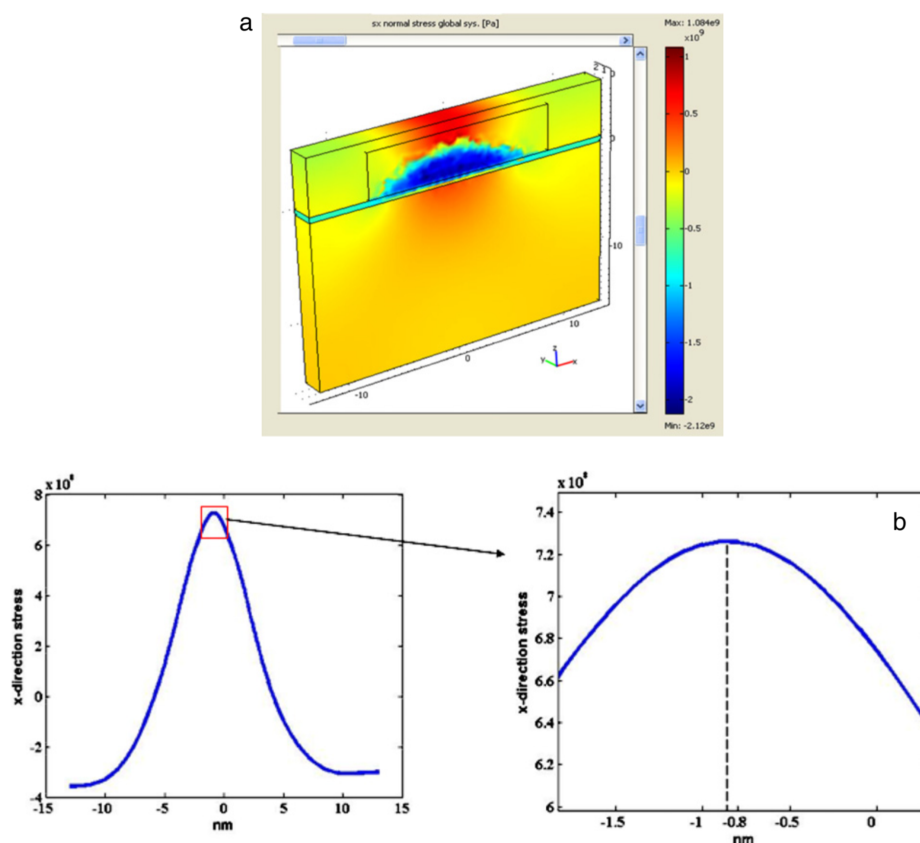

Figure 7. (a) 3D representation of the x [110] component of the stress (σ_{xx}, units: Pa) obtained by finite element calculations. Profiles of the σ_{xx} values versus x obtained at the surface of the 5 nm thick InP capping layer are shown in (b). The 0 nm point in the abscissa axis corresponds to the centre of the wire underneath. $x = [110]$; $y = [\bar{1}10]$; $z = [001]$.

zones that will favour nucleation of wires on the InP surface valleys [19]. However, the influence of the term μ_{S} can be considered negligible because local bending at the surface was not detected in our previous experimental AFM results (not shown) at the surface of a 5 nm thick InP cap layer. In this way the relevant term for surface chemical potential variations is μ_{E}.

These considerations let us propose, taking into account the position of the strain and stress critical values shown in figures 6 and 7, that preferential nucleation of wires on the InP capping layer surface will occur at x positions displaced some few lattice interplanar distances, around four (220) interplanar spacings in our case, with respect to the position located just on the centre of the wire underneath. The output of the finite element calculation using the asymmetrical compositional map to represent the wire therefore determines the existence of preferential nucleation on the capping layer surface at a distance (along [110]) of 0.86 nm from the central position of the wire underneath. In terms of α, the 5 nm capping layer surface has a preferential nucleation line located at an predicted angle of 9.8°, in good agreement with the experimental angle $\alpha = 9° \pm 5°$.

6. Conclusions

In conclusion, the determination of the strain and stress fields generated on an InAs(P) self-assembled wire capped with a 5 nm InP layer has been performed by means of finite element methods considering anisotropic elastic theory. We use as input parameter the As composition map experimentally obtained by electron energy loss spectroscopy spectra and high-resolution Z contrast imaging corrected for spherical aberration. Preferential sites of nucleation of stacked wires have successfully been located from the determined strain and stress fields by finding the growth surface zones where the chemical potential is minimized. Good agreement is found between the predicted and the experimental locations of the preferential sites for wire nucleation.

Acknowledgments

This work was supported by the SANDiE European Network of Excellence (Contract No NMP4-CT-2004-500101), the MEC NANOSELF II project (TEC2005-05781-C03), the CAM: S_0505ESP_0200 project, the Junta de Andalucia (PAI research group TEP-0120; project PAI05-TEP-00383) and by the Office of Basic Energy Sciences, Division of Materials Sciences and Engineering, US DOE, under contract DE-AC05-00OR22725 with ORNL, managed and operated by UT-Battelle, LLC.

References

[1] Nötzel R and Haverkor J E M 2006 *Adv. Funct. Mater.* **16** 327–34

[2] Benoit J M, Le Gratiet L, Beaudoin G, Michon A, Saint-Girons G, Kuszelewicz R and Sagnes I 2006 *Appl. Phys. Lett.* **88** 041113
[3] Michon A, Saint-Girons G, Beaudoin G, Sagnes I, Largeau L and Patriarche G 2005 *Appl. Phys. Lett.* **87** 253114
[4] Cornet C, Levallois C, Caroff P, Folliot H, Labbe C, Even J, Le Corre A, Loualiche S, Hayne M and Moshchalkov V V 2005 *Appl. Phys. Lett.* **87** 233111
[5] Skolnick M S and Mowbray D J 2004 *Ann. Rev. Mater. Res.* **34** 181–218
[6] González L, García J M, García R, Briones F, Martínez-Pastor J and Ballesteros C 2000 *Appl. Phys. Lett.* **76** 1104
[7] Lei W, Chen Y H, Wang Y L, Huang X Q, Zhao Ch, Liu J Q, Xu B, Jin P, Zeng Y P and Wang Z G 2006 *J. Cryst. Growth* **286** 23–7
[8] Lei W, Chen Y H, Wang Y L, Xu B, Ye X L, Zeng Y P and Wang Z G 2005 *J. Cryst. Growth* **284** 20–7
[9] Parry H J, Ashwin M J, Neave J H and Jones T S 2005 *J. Cryst. Growth* **278** 131–5
[10] Zhi C Y, Bai X D and Wang E G 2004 *Appl. Phys. Lett.* **85** 1802–4
[11] Krishnamachari U, Borgstrom M, Ohlsson B J, Panev N, Samuelson L, Seifert W, Larsson M W and Wallenberg L R 2004 *Appl. Phys. Lett.* **85** 2077–9
[12] Garcia J M, Gonzalez L, Gonzalez M U, Silveira J P, Gonzalez Y and Briones F 2001 *J. Cryst. Growth* **227/228** 975–9
[13] Fuster D, Gonzalez L, Gonzalez Y, Martinez-Pastor J, Ben T, Ponce A and Molina S I 2004 *Eur. Phys. J.* B **40** 434–7
[14] Fuster D, Gonzalez M U, Gonzalez L, Gonzalez Y, Ben T, Ponce A and Molina S I 2004 *Appl. Phys. Lett.* **84** 4723–5
[15] Ben T, Molina S I, Garcia R, Fuster D, González M U, González L, González Y and Kret S 2005 *Microscopy of Semiconducting Materials: Springer Proc. in Physics (Oxford, UK, April 2005)* (*Proc. 14th Conf.* vol 107) ed A G Cullis and A G Hutchison (London: Springer) pp 28–33
[16] Burenkov Yu A, Davydov S Yu and Nikanorov S P 1975 *Sov. Phys.—Solid State* **17** 1446 (http://www.ioffe.rssi.ru/SVA/NSM/Semicond/InAs/mechanic.html)
[17] Liu P, Zhang Y W and Lu C 2003 *Phys. Rev.* B **68** 195314
[18] Biasiol G and Kapon E 1999 *J. Cryst. Growth* **201/202** 62
[19] Ying B, Liu F and Lagally M G 2004 *Phys. Rev. Lett.* **92** 025502